Thorium isotopes tracing the iron cycle at the Hawaii Ocean Time-series Station ALOHA

Christopher T. Hayes[a,*], Jessica N. Fitzsimmons[a,1], Edward A. Boyle[a], David McGee[a], Robert F. Anderson[b], Rachel Weisend[c] and Peter L. Morton[c]

[a]Department of Earth, Atmospheric and Planetary Sciences, Massachusetts Institute of Technology, Cambridge, MA
[b]Lamont-Doherty Earth Observatory of Columbia University, Palisades, NY
[c]Department of Earth, Ocean, and Atmospheric Science, Florida State University, Tallahassee, FL
[1]Now at Institute of Marine and Coastal Studies, Rutgers University, New Brunswick, NJ
*Corresponding author: cthayes@mit.edu

Abstract

The role of iron as a limiting micronutrient motivates an effort to understand the supply and removal of lithogenic trace metals in the ocean. The long-lived thorium isotopes (^{232}Th and ^{230}Th) in seawater can be used to quantify the input of lithogenic metals attributable to the partial dissolution of aerosol dust. Thus, Th can help in disentangling the Fe cycle by providing an estimate of its ultimate supply and turnover rate. Here we present time-series (1994-2014) data on thorium isotopes and iron concentrations in seawater from the Hawaii Ocean Time-series station ALOHA. By comparing Th-based dissolved Fe fluxes with measured dissolved Fe inventories, we derive Fe residence times of 6-12 months for the surface ocean. Therefore, Fe inventories in the surface ocean are sensitive to seasonal changes in dust input. Ultrafiltration results also reveal that Th has a much lower colloidal content than Fe, implicating a predominant role for sub-micron organic ligands specific to Fe, or possibly inorganic Fe colloids. In the deep ocean, Fe approaches a solubility limit while Th, surprisingly, is continually leached from lithogenic particles. This distinction in solubility suggests Th is not a good tracer for Fe in the deep (>2 km) ocean. While uncovering divergent behavior of these elements in the water column, this study finds that dissolved Th flux is a suitable proxy for the supply of Fe from dust in the remote surface ocean.

1. Introduction

Determination of the supplies of iron to the ocean is relevant to understanding Earth's climate and the ocean's ecology. Ocean storage of carbon dioxide is mediated by iron supply in large areas of the ocean where Fe is a limiting resource, both today (Moore et al., 2013) and during the ice ages (Martínez-García et al., 2014). Additionally, the marine distribution of diazotrophic phytoplankton that modulate the nitrogen cycle may be determined by Fe supply rates (Ward et al., 2013). Atmospheric dust is arguably the major source of Fe to the euphotic zone (Boyd et al., 2010; Conway and John, 2014; Jickells et al., 2005; Tagliabue et al., 2014). Debate on the sources of marine Fe ensues largely because the techniques to estimate the supply rate of Fe from dust in particular, or Fe residence times in general, are only beginning to be developed.

In this study, we assess the utility of thorium isotopes in seawater to provide rate information on the Fe cycle. In addition to producing a measure of total dust flux to the ocean (Deng et al., 2014; Hsieh et al., 2011), by pairing ^{232}Th, sourced from dust, with radiogenic ^{230}Th (or ^{234}Th) that provides a timescale of thorium flux, one can make quantitative estimates of the trace metals released by dust dissolution (Hayes et al., 2013a). Our study site is the Hawaii Ocean Time-series station ALOHA (22° 45' N, 158° W) (Church et al., 2013; Karl and Lukas, 1996) in the subtropical North Pacific, where Asian dust is deposited in spring (Boyle et al., 2005; Hyslop et al., 2013; Prospero et al., 2003). Presenting time-series data spanning 20 yrs (1994-2014), we demonstrate that the behaviors of Fe and Th in seawater are consistent with a variable dust source to the surface ocean. Thorium-based fluxes indicate that the residence time of dissolved Fe in the upper 125 m of the water column is less than one year. In the sub-surface

ocean (>250 m), the thorium and iron cycles begin to diverge considerably. These divergences reveal new insights into the marine geochemistry of these elements.

2. Background

2.1 Finding the timescale: thorium removal

The rate information on trace metal cycling that we seek is obtained by exploiting the natural radioactive disequilibrium between insoluble ^{230}Th and its soluble parent ^{234}U in seawater. The oceanic distribution of ^{234}U (half-life 245,620 yrs (Cheng et al., 2013)) is homogeneous within a few parts per thousand, as ^{238}U concentrations vary only with salinity (Owens et al., 2011) and ^{234}U/^{238}U ratios vary by less than 1 per mil (Andersen et al., 2010). Therefore, the decay of ^{234}U produces ^{230}Th at a known rate everywhere in the ocean. Due to its insolubility, thorium adsorbs onto sinking particulate matter, a process called scavenging, on a timescale of years, much faster than ^{230}Th decay (half-life 75,584 yrs (Cheng et al., 2013)).

Thus by comparing the amount of ^{230}Th that remains in seawater to the amount produced by U decay, one can calculate a removal timescale (Eq. 1, Fig. 1), or residence time (τ), of thorium in seawater. This technique is analogous to that used with a more commonly used flux tracer, the shorter-lived ^{234}Th (half-life 24.1 days). By the same principles, using its production rate from parent isotope ^{238}U, ^{234}Th inventories can also be used to determine the scavenging rate of Th in seawater (Buesseler et al., 1992; Coale and Bruland, 1985).

$$\tau_{Th}(z) = \frac{\int_0^z {}^{230}Th\, dz}{\int_0^z {}^{234}U * \lambda_{230}\, dz} \qquad \text{Eq. 1}$$

To meet the requirements of a steady-state assumption between source and removal terms, we calculate thorium residence times in an integrated sense, from the surface to a particular depth. Thus as one integrates deeper into the water column, the ^{230}Th inventories reflect longer timescales of removal. Residence times calculated in this way also neglect

dispersal fluxes by ocean circulation. Lateral gradients in oceanic ^{230}Th concentrations are generally small (Hayes et al., 2014), while large vertical gradients may make vertical fluxes significant, for instance due to upwelling (Luo et al., 1995).

2.2 Finding the source: lithogenic metal fluxes

The dominant isotope of seawater thorium is primordial and long-lived (half-life 14.1 x 10^9 yrs) ^{232}Th. It is added to the ocean only through the partial dissolution of continental material, which in the context of station ALOHA we consider to be primarily aerosol dust. As scavenging tendencies are characteristic of all isotopes of an element, once in the water column, ^{232}Th undergoes scavenging removal (Fig. 1) assumedly at the same rate, i.e. with the same residence time, as ^{230}Th (or ^{234}Th). Assuming a steady-state for Th concentrations, with knowledge of the Th residence time, derived from ^{230}Th, one can calculate the flux of dust-derived ^{232}Th necessary to support the observed ^{232}Th inventory (Eq. 2). As in calculating thorium residence times, the dissolved ^{232}Th flux derived is reflective of the integrated depth zone, rather than at a particular depth. More details on ^{232}Th flux calculations are reported by Hayes et al. (2013a).

$$^{232}Th\ flux(z) = \frac{\int_0^z {}^{232}Th\ dz}{\tau_{Th}(z)} \qquad \text{Eq. 2}$$

In comparison to the relative simplicity of the supply and removal terms in the thorium cycle, seawater iron cycling has many more terms to consider. These include biological uptake, remineralization, redox chemistry, anthropogenic or hydrothermal sources, in addition to supply by dust and removal by scavenging (Fig. 1). Scavenging of Fe also occurs but at a different rate than that of Th. The utility of this element pair is their common source from dust. We propose using dissolved ^{232}Th flux as a proxy for the Fe released during dust dissolution. This can be

done with knowledge of the Fe/Th ratio in the dust and the relative fractional solubility of the two elements ($S_{Fe/Th}$, Eq. 3).

$$\text{Dust-dissolved Fe flux} = \text{dissolved } ^{232}\text{Th flux} \times (\text{Fe/Th})_{dust} \times S_{Fe/Th} \quad \text{Eq. 3}$$

By weight, the Asian desert dust which undergoes long-range transport over the North Pacific contains ^{232}Th at 14.3 ± 0.8 ppm, based on fine grained (<8 µm) source materials (McGee, 2009; Serno et al., 2014), and Fe at 3.8 ± 0.4 %, based on a literature compilation by Mahowald et al. (2005). Therefore, we assume the Fe/Th ratio in dust at station ALOHA of 2660 ± 320 g/g or 11,040 ± 1450 mol/mol. These ratios are close to the average for the upper continental crust of Fe/Th = 3271 g/g = 13,553 mol/mol (Taylor and McLennan, 1995).

The relative fractional solubility of Fe and Th in dust is currently unconstrained. Hayes et al. (2013a) assumed $S_{Fe/Th} = 1$ as a starting point, based solely on the similarly insoluble nature of these two elements in seawater. While much more work is needed to constrain this parameter, here we continue to assume $S_{Fe/Th} = 1$, and our observations of the time-series variability in the seawater Fe/^{232}Th ratio (section 4.4) support this assumption.

2.3 Iron residence times

We cannot rule out significant marine Fe sources by anthropogenic (e.g., derived from fossil fuel combustion) aerosols, continental margin sediments, or deep-sea hydrothermal vents. We can, however, entertain the thought that if dust were the only Fe source to the water column, the comparison between measured dissolved Fe inventories to the source (dust-dissolved Fe flux) would produce a measure of the turnover rate or residence time of dissolved Fe in seawater (Eq. 4). This residence time again represents the residence time within the integrated water column. Additional sources of Fe, such as combustion aerosols or hydrothermal fluids, would cause the

dust-based Fe residence time to be an overestimate. Relevant to iron cycling, this residence time provides a rough timescale over which one can expect Fe concentration to vary as a result of variation in sources, such as springtime Asian dust events (Boyle et al., 2005).

Dissolved Fe residence time = Fe inventory ÷ dust-dissolved Fe flux Eq. 4

3. Materials and Methods

3.1 Sample collection during 2012-2014

Samples were collected on several cruises on the R/V *Kilo Moana*, led by the Center for Microbial Oceanography: Research and Education (C-MORE), to station ALOHA in July-September 2012 (HOE-DYLAN), May-June 2013 (HOE-PhoR-I), September 2013 (HOE-PhoR-II) and March 2014 (HOE-BOE-I). Depth profiles for $^{230}Th/^{232}Th$ analysis were collected from the ship's Niskin bottle rosette, filtered with a 0.45 µm Acropak cartridge filter, and acidified to pH 1.8 with Savillex-distilled 6 M HCl.

Filtered surface seawater (0.4 µm) was collected for ^{232}Th (which requires smaller volumes than for ^{230}Th), as well as for dissolved Fe, using the trace-metal clean MITESS sampler (Bell et al., 2002) at near daily time intervals on the 2012-2013 C-MORE cruises. MITESS collection methods, including "Vane" sampling for Fe depth profiles, on the HOE campaigns are discussed fully by Fitzsimmons et al. (submitted). Within 3 hours of collection, the seawater was filtered using 0.4 µm polycarbonate track etch filters (PCTE, Whatman). Particulate samples were immediately frozen, and dissolved filtrates were acidified to pH 2 with trace metal clean HCl. The filters used for filtering MITESS water were analyzed for particulate Fe and ^{232}Th (representing on average 0.7 liters of seawater).

On HOE-PhoR-II, cross flow filtration was performed to assess colloidal $^{232}Th/^{230}Th$ using protocols developed to study colloidal Fe (Fitzsimmons and Boyle, 2014a). Seawater was

pre-filtered at 0.45 µm and, within 1-2 hours, pumped over a Millipore Pellicon XL filter made of regenerated cellulose with a nominal molecular weight cutoff of 10 kDa, roughly equivalent to an effective pore size of 10 nanometers. Both permeate and retentate fractions were analyzed to determine any loss of Th by adsorption, which turned out to be minimal (88-100% dissolved Th recovery).

3.2 Hawaii Ocean Time-series (HOT) seawater

Seawater samples, typically 0.5 liter size, have been collected during the HOT program for trace metal analysis at MIT periodically since 1997. Most of these samples were collected as unfiltered water using the MITESS sampler (Bell et al., 2002) and subsequently preserved by acidification to pH 2 with HCl. Further sampling details are given by Boyle et al. (2005). We also make use of literature seawater $^{232}Th/^{230}Th$ data, collected at station ALOHA in September 1994 (HOT-57), reported by Roy-Barman et al. (1996).

3.3 Thorium and iron analyses

Dissolved ^{230}Th concentrations at station ALOHA are as low as 10^{-18} moles per kilogram seawater (10^{-18} mol ^{230}Th = 0.1746 µBq). Therefore, for measurement by inductively-coupled plasma mass spectrometry (ICP-MS), 4-5 liter water samples are required. Thorium concentrations were determined by isotope dilution by spiking with ^{229}Th (not present in natural seawater). Sample preparation (pre-concentration, acid digestion, and chromatographic purification) was performed using published methods (Anderson et al., 2012; Auro et al., 2012). A portion of the ^{230}Th samples were prepared and analyzed at the Lamont-Doherty Earth Observatory (L-DEO), using an Element XR single-collector ICP-MS. The remaining ^{230}Th samples were prepared at the Massachusetts Institute of Technology (MIT) and analyzed using a

Neptune Plus multi-collector ICP-MS at Brown University. Th-232 was also analyzed in samples prepared for ^{230}Th.

Analysis of ^{232}Th, at 10^{-15} mol or femtomoles per kg seawater, required smaller samples (200-800 mL) and was measured on archive HOT and HOE samples for which sample volume did not allow ^{230}Th determination. While not as prone to contamination as some other trace elements, clean lab techniques were required to produce blanks that were consistent and low enough to allow detection of the relatively small sample size of ~20-40 femtomoles ^{232}Th. Therefore, modifications of the cited procedures for Th analysis (Anderson et al., 2012; Auro et al., 2012) were made. Instead of co-precipitation with added Fe, pre-concentration of ^{232}Th was achieved using magnesium hydroxide co-precipitation, such as that described for Pb by Reuer et al. (2003). Thorium was purified using a smaller amount (100 µl rather than 1 ml) of anion-exchange resin (AG1-X8) on columns fashioned from Teflon shrink-tubing. Samples were loaded onto AG1-X8 resin in 8 M HNO_3 and Th was eluted with 6 M HCl (instead of 12 M HCl, to reduce acid blank), following Edwards et al. (1987). Blank determinations were made on 125 mL aliquots of acidified seawater samples whose ^{232}Th content had been determined during previous ^{230}Th analysis. The mean procedural blank (n = 6) was 3.5 ± 1.6 fmol ^{232}Th, resulting in a detection limit of 4.8 fmol ^{232}Th. Samples for seawater ^{232}Th were prepared and analyzed at MIT, using a Micromass IsoProbe multi-collector ICP-MS.

In this study, we refer to measured trace metal concentrations as dissolved (filtered at 0.4 or 0.45 µm), particulate (>0.4 µm), or total (acidified unfiltered water). The "total" concentrations in this sense are sometimes referred to as "total dissolvable", allowing for the possibility that some forms of Th are not preserved by acidification or collected with co-precipitation. Since our goal in interpreting seawater ^{230}Th concentrations is to determine

scavenging rates based on uranium decay, we made small (0-10%) corrections for the dissolved ^{230}Th released from dust (or lithogenic material in general). This correction is based on measured dissolved ^{232}Th and a lithogenic ^{230}Th/^{232}Th mole ratio of 4 x 10^{-6} (Roy-Barman et al., 2009). The corrected dissolved ^{230}Th values are denoted as "xs".

Particulate ^{232}Th and particulate Fe, were analyzed at Florida State University by total digestion of the filter samples and subsequent analysis by ICP-MS, using slightly modified versions of published protocols (Ho et al., 2011; Morton et al., 2013; Upadhyay et al., 2009). In brief, samples were microwaved (CEM MARS Xpress) for 40 minutes at 180°C with HNO_3 and H_2O_2 (to digest the organic and less refractory biogenic and authigenic components) and HF (to digest the more refractory lithogenic components). The detection limit (based on 3 standard deviations of the digested acid blanks) for particulate ^{232}Th was 8 fmol/L (n=19) and the particulate Fe detection limit was 0.2 nmol/L (n=21). Dissolved Fe was measured by isotope dilution after pre-concentration onto nitrilotriacetate resin on the Micromass IsoProbe ICP-MS at MIT (Lee et al., 2011). Further details on Fe analyses are discussed by Fitzsimmons et al. (submitted).

Data presented in this study can be accessed in the Supplemental Material online.

4. Results and Discussion

4.1 ^{230}Th-^{232}Th depth profiles to 1.5 km

We focus first on the 2012-2013 thorium isotope depth profiles in the upper 1.5 km of the water column for a sense of the type of data used to calculate thorium fluxes (Fig. 2). High resolution depth profiles were analyzed in late July 2012, early June 2013 and late September 2013. The mixed layer depths during these sampling casts (based on 0.125 kg/m^3 density change)

were 54, 33 and 53 m, respectively, and below 100 m these profiles displayed little distinguishing hydrography (Figs. 2C, 2D, 2E).

For dissolved ^{232}Th (Fig. 2A), there were increased concentrations near the surface, minimum concentrations at the depth of maximum chlorophyll concentration (the DCM, ~120-140 m), and a relatively constant local concentration maximum at 500-600 m depth. At intermediate depths (900-1200 m), each profile exhibited smooth variations in concentration but concentrations at the different sampling dates vary by up to 30%.

The surface ^{232}Th maxima are consistent with aerosol dust as the major source of ^{232}Th to station ALOHA, as recognized by Roy-Barman et al. (1996). An interesting feature of these high-depth resolution measurements is that the surface (5 m) ^{232}Th concentration was lower than that in the core of the mixed layer (25 m depth) at these three sampling times. This is perhaps related to small-scale scavenging and export dynamics, or particle cycling in general.

The coincidence of the subsurface chlorophyll maximum and the minimum in ^{232}Th is apparently a universal feature for lithogenic trace elements such as Al, Ti and Fe (Dammshäuser et al., 2013; Fitzsimmons and Boyle, 2014b; Fitzsimmons et al., in press; Ohnemus and Lam, in press). This was also true for dissolved and particulate Fe at Station ALOHA during this study (Fitzsimmons et al., submitted). Increased particle aggregation efficiency, through the formation of fecal pellets, may more efficiently scavenge dissolved ^{232}Th from this depth.

Scavenged ^{232}Th may be partially released through remineralization of particles in mesopelagic depths (300-500 m). Thus remineralization may be responsible for some of the subsurface ^{232}Th maxima at 400-600 m depth. In support of this view, this depth range coincides with a rapid increase in phosphate concentration and apparent oxygen utilization, as inferred from HOT climatology (http://hahana.soest.hawaii.edu/hot/trends/trends.html). On the other

234 hand, the attenuation of particulate organic carbon at station ALOHA is most intense at
235 shallower depths, between 100 and 200 m (Bishop and Wood, 2008).
236 The dominant basalts of the Hawaiian Islands (tholeiitic) are low in Th content, 0.8 ± 0.4
237 ppm, according to available data in PetDB (www.earthchem.org/petdb) (Lehnert et al., 2000).
238 Nonetheless, with our seawater observations, we cannot fully rule out lateral input of Th from
239 the Hawaiian Islands. For instance, dissolved Mn concentrations reach a maximum near 800 m
240 depth at station ALOHA (Boyle et al., 2005) that may reflect a coastal source of metals.
241 The variability in ^{232}Th concentration at intermediate depths (900-1400 m) could be due
242 to the effect of hydrothermal activity at the nearby Loihi seamount. The iron oxide particles
243 associated with hydrothermal plumes strongly scavenge Th, and depleted deep-sea Th
244 concentrations have been observed up to 1400 km away from a vent site in the Atlantic (Hayes et
245 al. 2014). We note however, that while variability in ^{232}Th could suggest hydrothermal
246 scavenging, intriguingly, this effect is apparently weak enough to not significantly perturb the
247 near-linear ^{230}Th profiles (Fig. 2). Time-variability in the influence of the Loihi hydrothermal
248 system on trace metals at ALOHA is discussed more fully by Fitzsimmons et al. (submitted).
249 The ^{230}Th profiles also displayed interesting temporal variations. The theory of reversible
250 scavenging contends that a steady-state is achieved between thorium adsorption and desorption
251 on uniform particles that settle at a constant rate (Bacon and Anderson, 1982). Under these
252 assumptions, one expects ^{230}Th concentrations to increase linearly with depth with a boundary
253 condition of zero concentration at the surface. While the observed depth profiles are essentially
254 linear (Fig. 2B), it appears that mixing at the surface homogenizes ^{230}Th concentrations to some
255 depth. Interestingly, the layer of relatively homogeneous ^{230}Th extends deeper than the density-
256 defined mixed layer (30-50 m), down to the deep chlorophyll maximum (Fig. 2). This

257 phenomenon is worthy of future time-series study. Potentially a remnant of deep winter mixed
258 layers (< 100 m), the homogeneous surface ^{230}Th layer could also represent some combination
259 of vertical mixing and enhanced scavenging related to export of organic matter from the euphotic
260 zone.

261 Another significant observation is that while the surface ^{230}Th concentrations from June
262 and September 2013 were nearly identical (1.2 µBq/kg), the surface ^{230}Th concentrations from
263 July 2012 were about a factor of 2 lower (0.6 µBq/kg). This implies a relatively rapid change in
264 scavenging and/or export production. Future time-series studies are warranted to further assess
265 the short-term (daily-monthly) variability in euphotic zone ^{230}Th concentrations and how closely
266 these changes can be correlated with organic matter export. In the next section, we assess what
267 changes in the removal timescale are implied by these results.

268 *4.2 Surface thorium residence times*
269
270 Residence times of dissolved ^{230}Th as described in section 2.1 using the 2012-2014
271 results are presented in Figure 3. In this assessment, we integrate production due to ^{234}U decay
272 (based on salinity) and the measured ^{230}Th inventory to 150 m depth. This allows comparison to
273 Th residence times calculated on the basis of ^{234}Th:^{238}U disequilibrium established by previous
274 work at station ALOHA, during April 1999-March 2000 (Benitez-Nelson et al., 2001) and June-
275 July 2008 (Buesseler et al., 2009). The ^{234}Th results differ slightly from the approach used here
276 for dissolved ^{230}Th since the ^{234}Th fluxes are calculated using unfiltered seawater. Since
277 adsorbed ^{230}Th concentrations are on the order of ~10-20% of total ^{230}Th (Roy-Barman et al.,
278 1996), residence times based on total ^{234}Th can be expected to be up to 10-20% lower than those
279 based on the dissolved phase only.

We also assessed the influence of vertical mixing on surface ^{230}Th inventories, which could influence the derived residence time. Assuming a vertical mixing coefficient (K_v) of 10^{-5} m^2/s (Charette et al., 2013), using a second-order polynomial regression of the ^{230}Th depth profiles (above 250 m), we can calculate the vertical mixing rate of ^{230}Th, as $K_v \times d^2Th/dz^2$. The results indicate that vertical mixing adds ^{230}Th to surface water at a rate of less than 5% of production due to ^{234}U decay. Therefore we can assume that vertical mixing does not significantly affect the ^{230}Th residence time estimates at Station ALOHA.

Nearly all of the thorium residence time estimates fall in the range of 1 to 3 years with no significant seasonal cycle (Fig. 3). In the HOT climatology, organic carbon export at 150 m is highest in May-August. While export seasonality is relatively weak in this oligotrophic, subtropical location (Church et al., 2013), long-term monitoring has revealed episodic export events related to diatom blooms and symbiotic cyanobacteria, typically in late July and early August (Karl et al., 2012).

The concept of "residence time" used here is based on a steady-state assumption for sources and sinks. Therefore with a residence time of ~2 years, one would not expect significant variation in the removal timescale over a period of months. However, the range in observed Th residence times for Station ALOHA indicates that this steady-state assumption is not quite correct. More precisely, the steady-state for scavenging removal of Th appears to hold within a factor of 2-3. The range in removal timescales observed based on ^{230}Th is similar to that based on ^{234}Th. Thus, it seems the rate of thorium scavenging can change dynamically at Station ALOHA possibly related to export pulses, but the data are consistent with a long-term average thorium residence time of 2 ± 1 years in the upper 150 m.

4.3 Surface ^{232}Th concentrations

303 With relatively good control on the removal timescale of thorium, we turn to observed
304 variability in surface ^{232}Th concentrations. Barring significant fluxes due to lateral circulation,
305 this variability represents the balance between removal by scavenging and input by dust. Smaller
306 volume requirements for analysis (<1 liter) allowed us to investigate ^{232}Th from daily, monthly
307 and decadal timescales.
308 Collected during a series of cruises in summer 2012 (HOE-DYLAN), daily-scale samples
309 of 250 mL were analyzed for dissolved and particulate ^{232}Th. Sample size required combining
310 the samples from 2-4 days for dissolved ^{232}Th, contributing to some degree of smoothing.
311 Dissolved concentrations ranged from 45-90 fmol/kg (Fig. 4C). Particulate ^{232}Th, although
312 measured at a higher, daily resolution, had a higher range of variability, from 10-290 fmol/kg. Of
313 the total seawater ^{232}Th (dissolved + particulate) during HOE-DYLAN, on average 42% was in
314 the particulate phase (range 26-66%). This fraction particulate is higher than that for ^{230}Th
315 (~15%, Roy-Barman et al., 1996) since particulate ^{232}Th represents both adsorbed Th and
316 structural Th in mineral dust.
317 The decadal time-series observations (1994-2014) of total ^{232}Th (Fig. 4A) exhibit a range
318 in concentration (~50-300 fmol/kg) that is consistent with the higher frequency observations of
319 particulate Th in 2012-2013. Since most of the data fall within the range of 50-150 fmol/kg, we
320 are not fully confident in the five observations of elevated concentrations (150-300 fmol/kg)
321 observed in 1994, 1998, and 1999 samples. In particular, the 1998 and 1999 samples were
322 collected using a moored, rather than ship-based, MITESS sampler in which bottles were filled
323 with 1 M HCl prior to filling with seawater. Mooring-collected water at times had higher Th
324 concentrations than ship-based sampling (Fig. 4) and thus the possibility of contamination during
325 sampling, sample storage, or sample analysis cannot be fully discounted. In fact, the 1994 results

from Roy-Barman et al. (1996) came from samples collected on the same Niskin bottle cast. Spatial variability, related to mesoscale eddies, is another potential source of rapid changes in surface ^{232}Th concentration. Conservatively excluding the elevated observations >150 fmol/kg, no significant temporal term trend can be derived.

When all observations are placed on a monthly axis (Fig. 4B), there is a hint that elevated surface ^{232}Th concentrations are observed during the spring (Mar-Jun) season of Asian dust transport over the North Pacific. It appears that dissolved ^{232}Th may be relatively constant throughout the year, consistent with the Th residence times of ~2 yrs derived in section 4.2. Unfortunately, few observations of dissolved ^{232}Th have been yet made during the spring season when dust input can increase by 2 orders of magnitude (Hyslop et al., 2013). Of course, these data are sparse, but they do provide a baseline of variability against which future trace metal observations can be measured.

4.4 *Fe/Th ratio behavior in surface water and in colloidal content*

Before applying the ^{232}Th flux technique, comparison of the time-series behavior of Fe (Fitzsimmons et al., submitted) and ^{232}Th is informative in terms of relative solubility and relative removal rates (Fig. 5). This is possible because both elements have been analyzed on the same samples from HOE-DYLAN, HOE-PhoR and many of the HOT archive samples.

In the context of daily, monthly and decadal variability, it appears that the ratio of total and particulate Fe/^{232}Th tends to be at or above the dust-ratio of 11,040 mol/mol, while dissolved Fe/^{232}Th is at or below the dust-ratio (Fig. 5A & 5B). These observations are consistent with input at the dust Fe/^{232}Th ratio and a strong sink from biological uptake for Fe. Thus, the dissolved phase is left depleted in Fe relative to ^{232}Th, while the particulate phase becomes enriched in biogenic Fe. The total Fe/Th ratio often exceeds the dust ratio as well, possibly

because biogenic particulate Fe may be efficiently recycled and thus may reside in the surface longer than particulate Th.

The partitioning between dissolved and total/particulate Fe/^{232}Th centers around the dust-ratio (Fig. 5C). We interpret this to mean that the relative fractional solubility of Fe and ^{232}Th ($S_{Fe/Th}$) is close to 1. An alternate interpretation would be that ^{232}Th is more efficiently leached from dust, leaving the particulate phase enriched in Fe/^{232}Th and the dissolved phase depleted in Fe/^{232}Th. However, given the known ability for phytoplankton to efficiently utilize Fe from dust sources (e.g., (Rubin et al., 2011)), the assumption of $S_{Fe/Th} = 1$ during dissolution followed by rapid biological uptake of Fe seems more likely.

Consideration of the size-partitioning of Fe and Th within the dissolved phase provides another constraint on the pathways these elements take after being released by dust. This investigation was also used as an opportunity to determine whether ^{232}Th and ^{230}Th have coherent speciation, as assumed for the ^{232}Th flux method. Figure 6 presents these results based on measurements of ultra-filtered seawater from HOE-PhoR-II in September 2013. We define colloidal Th as dissolved (< 0.45 µm) minus soluble (< 10 kDa).

Of the measured dissolved Th, less than 25% was found in the colloidal phase (0.45 µm-10 kDa ≈ 0.01 µm). Furthermore, at least at 15 m, 130 m (DCM), and 1000 m, the colloidal percentage for ^{232}Th and ^{230}Th agreed within the uncertainty of the measurements. This result implies coherent speciation of these thorium isotopes despite very different sources and supports the use of ^{230}Th as a tracer for ^{232}Th removal. This coherent speciation result agrees with previous measurements of the ^{232}Th/^{230}Th ratio of filtered (< 0.2 µm) and ultrafiltered (< 1 kDa) solutions from the Mediterranean Sea (Roy-Barman et al., 2002).

371 The role of colloids in Th scavenging has much history and deserves a few words of
372 context. Early models of scavenging inferred that Th likely goes through a colloidal intermediate
373 before being scavenged by larger, sinking particles (Honeyman et al., 1988; Honeyman and
374 Santschi, 1989). Subsequent attempts at measuring colloidal Th focused largely on ^{234}Th (see
375 review by (Guo and Santschi, 2007)), in part due to its use in quantifying organic matter export.
376 A generalization might be made that outside of the coastal ocean, colloidal ^{234}Th was found to be
377 relatively small (~<15%) proportion of the total dissolved (e.g., (Guo et al., 1997; Huh and Prahl,
378 1995; Moran and Buesseler, 1992)), which is also consistent with our ^{230}Th/^{232}Th results. Recent
379 observations from the North Atlantic (Hayes et al., submitted), however, observed scavenging
380 characteristics consistent with a strong role for Th colloids as predicted by Honeyman and
381 Santschi (1989), even at open-ocean particle concentrations of < 10 µg/kg seawater. Further
382 observations on the geographic distribution of colloidal Th are clearly warranted.
383 Our paired observations of Th and Fe size partitioning nonetheless provide additional
384 information on their physicochemical speciation in a comparative sense. Dissolved Fe has much
385 more colloidal content at ALOHA than Th (Fig. 6). Above the DCM, dissolved Fe can be >50%
386 colloidal. In the deeper water column, to 1.5 km depth, colloidal Fe is relatively constant at 40%
387 (with the exception of one sample < 10% colloidal at 650 m). Since Fe and ^{232}Th are apparently
388 solubilized from dust with equal fractional solubility, this difference in size-speciation is most
389 likely also due to the selective uptake or complexation of Fe by organic substrates. Ligands, in
390 the form of macromolecular organic molecules or organic colloidal particles, most likely
391 complex Fe released from dust quite rapidly in the upper water column (Bressac and Guieu,
392 2013; Mendez et al., 2010). It is the size of these organic Fe-binding ligands that are thought to
393 convert such a large percentage of dissolved Fe to colloidal size, as other similarly hydrolyzable

metals such as Al and Ti do not have significant colloidal components (Dammshäuser and Croot, 2012).

Similar to Al and Ti, the abundance of macromolecular ligands (>10 kDa) with an affinity to complex Th must also be small compared to the source of dissolved Th from dust. This finding does not necessarily contradict previous evidence for significant organic complexation of Th in seawater (Santschi et al., 2006). It does require, however, that any significant Th complexation is done by small (<10 nm), low-molecular weight organic molecules, at least at station ALOHA.

Greater uptake of Fe into the colloidal phase is another piece of evidence that suggests that dissolved Fe is cycled more rapidly than Th in the upper water column. The innovation of the ^{232}Th flux method is our ability to be quantitative about the rates of Fe removal, which are presented in the next section.

4.5 Iron residence times

Using the 2012-2013 Th profile data, we extend our calculations for Th residence time down to 1.5 km water depth in Fig. 7A. Beginning at the 1-2 years residence times calculated by integrating to the DCM, the Th residence times increase nearly linearly with integration depth to 14 years at 1.5 km. Dividing the integrated dissolved ^{232}Th inventories by these residence times gives our estimate of dissolved ^{232}Th flux, as function of integration depth, in Fig. 7B.

In June and Sept. 2013, the dissolved ^{232}Th flux increased with integration depth and begins to level-off around 500 m. This reflects that, at these times, the inventory of dissolved ^{232}Th increased with integration depth slightly more quickly than the increase in Th residence time with depth. Interestingly, in July 2012, the dissolved ^{232}Th flux decreased with integration depth, reflecting that the Th residence time increased more quickly than the dissolved ^{232}Th

inventory, largely because the mixed layer ^{230}Th concentrations were exceptionally low at this time. Estimated ^{232}Th fluxes are clearly quite sensitive to short-term variability in scavenging rates. We suggest further time-series analysis along with modelling efforts that contain circulation and realistic particle fluxes to determine more quantitatively the sensitivities involved in calculating dissolved ^{232}Th fluxes during moderate changes in scavenging rates and dust input.

The three flux profiles converge around 1000 m depth. This is encouraging that over longer integration times, 10-15 years in this case, we estimate consistent lithogenic metal fluxes at multiple time points. Using Eq. 1, the dissolved ^{232}Th fluxes are simply converted to dust-dissolved Fe fluxes, using $S_{Fe/Th} = 1$ and $(Fe/Th)_{dust} = 11{,}040$ mol/mol, shown in the second x-axis in Fig. 7B. The depth profiles of dissolved Fe concentrations from the same sampling campaigns are shown in Fig. 7C (Fitzsimmons et al., submitted). Finally, using Eq. 2, by integrating Fe inventories and dividing by the dust-dissolved Fe fluxes, we estimate the residence time of dissolved Fe, as a function of integrated depth in Fig. 7D.

In the upper 250 m, the residence time of dissolved Fe is 6 months to 1 year. This range agrees well with the 6 month residence time estimated previously at station ALOHA (Boyle et al., 2005), and with other estimates of surface ocean dissolved Fe residence times from the Atlantic based on measured Fe concentrations and assumptions about soluble aerosol deposition (Bergquist and Boyle, 2006; Jickells, 1999; Ussher et al., 2013). With such fast turnover times, dissolved Fe concentrations in surface waters can be expected to vary on monthly to yearly timescales with changes in the seasonal input of dust from Asia, which is exactly what was observed over the HOT and HOE time-series (Fitzsimmons et al., submitted).

Available aerosol data suggest that Asian dust transport over the North Pacific has no significant trend from 1981 to 2000 (Prospero et al., 2003) and perhaps a 6% decline over the

440 past 10 years (Hyslop et al., 2013). Because of a nearly immediate impact on surface water Fe
441 concentrations and the associated ecological consequences, it is important to monitor future
442 changes in Fe sources. Sources such as Asian desert dust in our changing climate may vary
443 independently of other Fe sources such as combustion aerosols.

444 As one integrates further from 250 m to 1500 m, while the dissolved Fe fluxes change
445 only moderately, the dissolved Fe residence times increase quickly to about 10 years at 1500 m
446 depth. This is due to the large increase in Fe concentrations at these depths due to
447 remineralization of Fe from sinking organic material and some portion of Fe accumulated and
448 transported to ALOHA laterally via deep ocean circulation. There is potentially additional input
449 of Fe at ~1 km depth due to Loihi hydrothermal activity. Additional lateral sources would cause
450 our dust-based dissolved Fe residence time to be an overestimate, implying even faster
451 timescales of Fe removal. On the other hand, as discussed in the next section, the 10 year Fe
452 residence time at 1500 m could indeed be an underestimate, if the geochemical cycles of Th and
453 Fe become decoupled at greater depths where dust dissolution is no longer a significant source of
454 dissolved Fe.

455 *4.6 Fe and Th decoupling in the deep ocean*

456 Our focus on the upper water column stems from our motivation to understand trace
457 metal cycling due to aerosol deposition and export production. We can extend our analysis of Fe
458 and Th into the deep ocean (4.5 km water depth at station ALOHA) to learn about the
459 geochemistry of these elements over decadal-to-centennial timescales. In Figure 8, we compiled
460 available deep profiles from station ALOHA for dissolved Fe (Boyle et al., 2005; Fitzsimmons et
461 al., submitted; Morton, 2010) and dissolved $^{232}Th/^{230}Th$ (this study; Roy-Barman et al. (1996)).

462 Variability in dissolved Fe at 1-1.5 km is clearly apparent, possibly due to hydrothermal
463 inputs. Below 1.5 km depth, Fe, ^{232}Th, and ^{230}Th display relatively constant profile shapes, at
464 least during the sparse sampling dates. From 2 km depth to the bottom, dissolved Fe is nearly
465 constant or slightly decreases with depth to about 0.5 nmol/kg, while dissolved ^{232}Th actually
466 increases with depth from 50 to 180 fmol/kg below 3000 m. This divergence in profile shape
467 already suggests a decoupling of the behavior of these elements in the deep ocean.
468 The deep ocean appears to contain an additional source for ^{232}Th. This source is
469 potentially related to resuspension of diagenetically-altered sediments at the seafloor (Hayes et
470 al., 2013a; Okubo et al., 2012). The bottom-increase in ^{232}Th begins nearly 2 km above the
471 seafloor, much high than typical benthic vertical mixed layers (50-100 m) (Richards, 1990). This
472 phenomenon, as observed with km-scale nepheloid layers (McCave, 1986), suggests that the
473 ^{232}Th at abyssal depths of station ALOHA is being mixed in laterally from locations where
474 isopycnals impinge on surrounding bathymetry.
475 Also related to bottom sediment resuspension, the July 2012 profile of ^{230}Th displays a
476 negative concentration anomaly, or deficit of ^{230}Th, with respect to the linear profile near the
477 seafloor (Fig. 8C). This bottom ^{230}Th deficit is indicative of enhanced bottom scavenging as
478 observed in many parts of the deep North Pacific (Hayes et al., 2013b; Okubo et al., 2012). It is
479 non-intuitive that in a bottom layer where the scavenging removal of Th is enhanced compared
480 to the overlaying water column, that this layer would also be a strong source of ^{232}Th. The
481 resuspension of bottom sediments may produce such a strong release of ^{232}Th that this source
482 more than compensates for enhanced scavenging.
483 Dissolved Fe, on the other hand, appears unaffected by bottom processes, displaying only
484 a slight decrease in concentration with depth (Fig. 8A). The slight decrease with depth may be

485 related to scavenging of Fe as deep water masses age (Bruland et al., 1994). If we extend our
486 integrated residence time approach to the deep Fe profile at station ALOHA (Fig. 9), we derive a
487 whole ocean residence for dissolved Fe of only 30 years. This is significantly shorter than the
488 100-300 year estimates of the ocean residence time for dissolved Fe based on deepwater
489 scavenging (Bergquist and Boyle, 2006; Bruland et al., 1994). This discrepancy arises most
490 likely because the deep ocean source of ^{232}Th does not add dissolved Fe to the water column at a
491 crustal ratio, unlike what occurs during dust dissolution. Thus, the ^{232}Th flux method for Fe
492 residence times cannot be extended to the deep ocean.

493 The question remains: how is an element like Th, a trace component of continental
494 material, added to the deep ocean without a simultaneous release of a major crustal element like
495 Fe? The answer is likely related to solubility.

496 Dissolved Fe in the deep central North Pacific at ~0.5 nmol/kg has been found to be at
497 near solubility equilibrium with Fe(III) hydroxide (Kitayama et al., 2009; Kuma et al., 2003).
498 These studies determine Fe(III) solubility by adding gamma-emitter ^{59}Fe(III) to filtered seawater,
499 allowing the solutions to come to solubility equilibrium with Fe(III) hydroxide over several
500 weeks, subsequently filtering the seawater and then counting the ^{59}Fe gamma-activity on the
501 final filtrate. The observed ~0.5 nmol/kg solubility is elevated over Fe solubility in inorganic
502 seawater because of the presence of organic ligands (Liu and Millero, 2002). Thus, since the
503 deep Pacific is in a near saturation state, dissolved Fe can no longer be expected to increase, even
504 in the presence of increasing Th concentrations.

505 A problem with this argument is that electrochemically-determined Fe ligand
506 concentrations at station ALOHA are up to 2 nmol/kg, well in excess of dissolved Fe
507 concentrations (Rue and Bruland, 1995), as found in most of the world ocean (Gledhill and

508 Buck, 2012). However, it may not be appropriate to compare Fe ligand determinations directly
509 with seawater solubility. In either estimation, deepwater dissolved Fe is at least close to (within
510 the same order of magnitude) our best estimates of Fe solubility.

511 While much less in known about Th solubility in seawater, our large underestimate of Fe
512 residence time in the deep ocean implies that the deep North Pacific, with Th at ~180 fmol/kg, is
513 not near Th solubility equilibrium. Near seawater pH and ionic strength, the solubility of Th(IV)
514 hydroxide may be as high as 0.5-1 nmol/kg, compared to 1 fmol/kg for crystalline ThO_2, due to
515 the amorphous nature of $Th(OH)_4$ solids (Neck et al., 2003). Despite our findings of low
516 colloidal Th content, electrochemical methods suggest organic Th ligands may also exist at
517 nanomolar concentrations (Hirose, 2004). Significant organic Th could of course be present at
518 station ALOHA if the complexes are smaller than ~10 nm. We advocate direct measurements of
519 Th solubility in seawater, perhaps using radio-tracer additions with similar protocols as
520 developed for Fe (Kuma et al., 1996; Schlosser and Croot, 2008), to confirm that Th exists in the
521 deep ocean at much less than its equilibrium solubility. This would explain the fact that
522 dissolved Th concentrations continue to grow from lithogenic sources in the deep North Pacific,
523 where Fe concentrations become fixed by a solubility limit.

524 **5. Conclusions**

525 Using time-series data from the North Pacific, this study finds variability in surface Fe
526 and ^{232}Th concentrations consistent with a source from Asian dust. The dust source likely has a
527 relative Fe/Th fractional solubility close to 1. The application of ^{230}Th scavenging rates to ^{232}Th
528 inventories allows the accurate prediction of the flux of dissolved metals from dust in the remote
529 surface ocean. The source flux of dissolved Fe, derived from ^{230}Th-based timescales, suggests
530 that dissolved Fe in the upper 250 m is turning over in 1 year or less. A compelling implication

of this result is that Fe delivery to phytoplankton can be expected to vary with seasonal-to-interannual changes in dust delivery from Asia. Continued monitoring of Fe-dependent biological processes, such as nitrogen fixation, are crucial to anticipate the consequences of changing land-use and/or industrial processes that may significantly affect eolian sources of Fe to the North Pacific. In addition, we hypothesize that iron reaches a solubility limit in the deep sea (>2 km) while Th does not, and the influx of Th cannot be used as a proxy for Fe sources in this environment. Thus, the kinetic box model approach to tracing dust-derived elements (Fig. 1) appears applicable only in the upper water column (~250 m).

Acknowledgements

We acknowledge funding from the W.O. Crosby Postdoctoral Fellowship to CTH and the National Science Foundation through C-MORE, NSF-OIA EF-0424599 to EAB, and NSF-DMR 1157490 supported RW and PLM. Soumen Mallick and Alberto Saal are thanked for facilitating mass spectrometry performed at Brown University. Major thanks go to Tara Clemente and Sam Wilson for their leadership roles on C-MORE cruises, and to Rick Kayser, Gonzalo Carrasco, Abigail Noble, Simone Moos, Mengli Chen, and Rene Boiteau for their help in collecting samples returned to MIT.

Figure Captions

Figure 1. Tracing the Fe cycle with the behavior of the long-lived thorium isotopes. Thorium-230 has a well-known source from the radioactive decay of its parent ^{234}U. This allows a quantitative estimate of Th removal due to scavenging on to particles. This removal rate can be used to estimate the steady-state source of ^{232}Th from the partial dissolution of aerosol dust. While Fe has many more terms in its biogeochemical cycling, its ultimate source from dust dissolution can be predicted using known ^{232}Th fluxes and the relative solubility of Fe and Th. Assuming Fe is derived only from dust, one can then estimate a maximum Fe residence time or minimum turnover rate.

Figure 2. Depth profiles from the Hawaii Ocean Time-series station ALOHA from sampling campaigns in 2012-2013. In July 2012 and June 2013, profiles for dissolved ^{232}Th (A) and ^{230}Th (B) were collected in two casts (shallow to 250 m and deep to 1500 m) on different days.

Relative uncertainty in isotope concentrations was 1-5% and thus errors bars would be close to the symbol size. The hydrographic profiles (C-F) are shown from the shallow cast only.

Figure 3. Thorium residence times, or turnover rates, calculated for the upper 150 m at station ALOHA on a monthly axis combining data from 1999 to 2014. These times are calculated by comparing integrated Th inventories to integrated production by uranium decay. The ^{234}Th-based results are reported by Buesseler et al. (2009) and Benitez-Nelson et al. (2001). Note the ^{230}Th-based results from March 2014 are not based on profiles but on single samples from 25 m, assuming uniform concentrations in the upper 150 as seen in the 2012-2013 profiles (Fig. 2).

Figure 4. Station ALOHA time-series data from the surface ocean (0-10 meters depth) on dissolved (filtered at 0.45 or 0.4 µm), total (unfiltered) and particulate (digested 0.4 µm filter) ^{232}Th in full time-series (1994-2014) (A), monthly climatology (1991-2014) (B) and during a daily resolution period in July-Sept. 2012 (C). Note change in scale of y-axes at 160 fmol/kg. Results from 1994 were reported by Roy-Barman et al. (1996). Open circles represent samples collected using a mooring rather than ship-based sampling (Sec. 4.1). Relative uncertainty in dissolved, total and particulate ^{232}Th concentrations was 1-10%.

Figure 5. Station ALOHA time-series data from the surface ocean (0-10 meters depth) (A), monthly climatology (B) and a daily resolution period in July-Sept. 2012 (C) of the dissolved (filtered at 0.45 or 0.4 µm), total (unfiltered) and particulate (digested 0.4 µm filter) Fe/^{232}Th ratio. Note change in scale of y-axes at 25,000 mol/mol. The dotted lines represent the Fe/^{232}Th ratio of Asian dust of 10,800 ± 1,200 mol/mol (1σ). Note in (C), four samples with particulate Fe/^{232}Th ratios greater than 40,000 are not shown. Open circles represent samples collected using a mooring rather than ship-based sampling (Sec. 4.1).

Figure 6. Depth profiles of the percentage of dissolved metals (<0.45 µm for Th or <0.4 µm for Fe) that are in the colloidal size fraction (roughly 10-400 nm) from station ALOHA in late September 2013. Colloidal content is estimated by subtracting the metal concentration in 0.4 µm filtered seawater (dissolved) from that passing through a 10 kDa membrane filter by cross-flow filtration (soluble). Colloidal fractions of ^{232}Th and ^{230}Th agree within uncertainties, while Fe colloidal content is 2-3 times larger.

Figure 7. Application of dissolved ^{232}Th fluxes to predict the residence time of dissolved Fe in seawater at station ALOHA during 2012-2013. Dissolved Th residence times (A) are calculated as a function of integration depth using radioactive disequilibrium between ^{234}U and ^{230}Th. The integrated ^{232}Th inventories divided by these residence times produces an estimate of the dissolved ^{232}Th flux (B) due to dust dissolution. Assuming equal fractional solubilities dissolution and a near crustal composition for Asian dust, the flux of dissolved Fe from dust can be predicted using the second x-axis in (B). The integration of dissolved Fe inventories based on concentration profiles shown in (C) (Fitzsimmons et al., submitted), produces our estimate of dissolved Fe residence time in (D, note change in scale of x-axis at 1.2 yrs).

Figure 8. Full ocean depth profiles from station ALOHA for dissolved Fe (A), ^{232}Th (B) and ^{230}Th (C) using data from this study (July 2012) and compiled from the literature. Iron data from

April 2001 and July 2002 were reported by Boyle et al. (2005) and from June 2002 by Morton (2010). Dissolved Th data from 1994 were reported by Roy-Barman et al. (1996). Note in (C) the dotted grey line is the linear regression of ^{230}Th data between 1 and 3.5 km, which when extended to the seafloor demonstrates that the bottom two samples are less than expected from reversible scavenging and imply enhanced scavenging (assuming no other processes affect supply and removal of ^{230}Th here).

Figure 9. Application of dissolved ^{232}Th fluxes to predict Fe residence times for the full depth ocean at station ALOHA. Here data from July 2012 are used to calculate ^{232}Th fluxes (A). The depth profiles of Fe concentrations presented in Fig. 8 were averaged to calculate the dissolved Fe residence times as a function of integration depth (B). The 30 year ocean residence for dissolved Fe is significantly lower than the century-scale residence times derived by other approaches, suggesting that ^{232}Th flux may not be an accurate proxy for Fe sources in the deep ocean.

References

Andersen, M.B., Stirling, C.H., Zimmermann, B. and Halliday, A.N. (2010) Precise determination of the open ocean ^{234}U/^{238}U composition. Geochem. Geophys. Geosyst. 11, Q12003.

Anderson, R.F., Fleisher, M.Q., Robinson, L.F., Edwards, R.L., Hoff, J., Moran, S.B., Rutgers van der Loeff, M.M., Thomas, A.L., Roy-Barman, M. and François, R. (2012) GEOTRACES intercalibration of ^{230}Th, ^{232}Th, ^{231}Pa, and prospects for ^{10}Be. Limnol. Oceanogr. Methods 10, 179-213.

Auro, M.E., Robinson, L.F., Burke, A., Bradtmiller, L.I., Fleisher, M.Q. and Anderson, R.F. (2012) Improvements to 232-thorium, 230-thorium, and 231-protactinium analysis in seawater arising from GEOTRACES intercalibration. Limnol. Oceanogr. Methods 10, 464-474.

Bacon, M.P. and Anderson, R.F. (1982) Distribution of thorium isotopes between dissolved and particulate forms in the deep sea. J. Geophys. Res. 87, 2045-2056.

Bell, J., Betts, J. and Boyle, E. (2002) MITESS: a moored in situ trace element serial sampler for deep-sea moorings. Deep-Sea Res. I 49, 2103-2118.

Benitez-Nelson, C., Buesseler, K.O., Karl, D.M. and Andrews, J. (2001) A time-series study of particulate matter export in the North Pacific Subtropical Gyre based on ^{234}Th:^{238}U disequilibrium. Deep-Sea Res. I 48, 2595-2611.

Bergquist, B.A. and Boyle, E.A. (2006) Dissolved iron in the tropical and subtropical Atlantic Ocean. Global Biogeochem. Cycles 20, GB1015.

Bishop, J.K.B. and Wood, T.J. (2008) Particulate matter chemistry and dynamics in the twilight zone at VERTIGO, ALOHA and K2 sites. Deep-Sea Res. I 55, 1684-1706.

Boyd, P.W., Mackie, D.S. and Hunter, K.A. (2010) Aerosol iron deposition to the surface ocean — Modes of iron supply and biological responses. Mar. Chem. 120, 128-143.

644 Boyle, E.A., Bergquist, B.A., Kayser, R.A. and Mahowald, N. (2005) Iron, manganese, and lead at
645 Hawaii Ocean Time-series station ALOHA: Temporal variability and an intermediate water hydrothermal
646 plume. Geochim. Cosmochim. Acta 69, 933-952.

647 Bressac, M. and Guieu, C. (2013) Post-depositional processes: What really happens to new atmospheric
648 iron in the ocean's surface? Global Biogeochem. Cycles 27, 859-870.

649 Bruland, K.W., Orians, K.J. and Cowen, J.P. (1994) Reactive trace metals in the stratified central North
650 Pacific. Geochim. Cosmochim. Acta 58, 3171-3182.

651 Buesseler, K.O., Bacon, M.P., Kirk Cochran, J. and Livingston, H.D. (1992) Carbon and nitrogen export
652 during the JGOFS North Atlantic Bloom experiment estimated from ^{234}Th:^{238}U disequilibria. Deep-Sea
653 Res. A 39, 1115-1137.

654 Buesseler, K.O., Pike, S., Maiti, K., Lamborg, C.H., Siegel, D.A. and Trull, T.W. (2009) Thorium-234 as
655 a tracer of spatial, temporal and vertical variability in particle flux in the North Pacific. Deep-Sea Res. I
656 56, 1143-1167.

657 Charette, M.A., Breier, C.F., Henderson, P.B., Pike, S.M., Rypina, I.I., Jayne, S.R. and Buesseler, K.O.
658 (2013) Radium-based estimates of cesium isotope transport and total direct ocean discharges from the
659 Fukushima Nuclear Power Plant accident. Biogeosciences 10, 2159-2167.

660 Cheng, H., Edwards, R.L., Shen, C.-C., Polyak, V.J., Asmerom, Y., Woodhead, J., Hellstrom, J., Wang,
661 Y., Kong, X., Spötl, C., Wang, X. and Calvin Alexander Jr, E. (2013) Improvements in ^{230}Th dating, ^{230}Th
662 and ^{234}U half-life values, and U–Th isotopic measurements by multi-collector inductively coupled plasma
663 mass spectrometry. Earth Planet. Sci. Lett. 371–372, 82-91.

664 Church, M.J., Lomas, M.W. and Muller-Karger, F. (2013) Sea change: Charting the course for
665 biogeochemical ocean time-series research in a new millennium. Deep-Sea Res. II 93, 2-15.

666 Coale, K.H. and Bruland, K.W. (1985) ^{234}Th:^{238}U disequilibria within the California Current. Limnol.
667 Oceanogr. 30, 22-33.

668 Conway, T.M. and John, S.G. (2014) Quantification of dissolved iron sources to the North Atlantic
669 Ocean. Nature 511, 212-215.

670 Dammshäuser, A. and Croot, P.L. (2012) Low colloidal associations of aluminium and titanium in surface
671 waters of the tropical Atlantic. Geochim. Cosmochim. Acta 96, 304-318.

672 Dammshäuser, A., Wagener, T., Garbe-Schönberg, D. and Croot, P. (2013) Particulate and dissolved
673 aluminum and titanium in the upper water column of the Atlantic Ocean. Deep-Sea Res. I 73, 127-139.

674 Deng, F., Thomas, A.L., Rijkenberg, M.J.A. and Henderson, G.M. (2014) Controls on seawater ^{231}Pa,
675 ^{230}Th and ^{232}Th concentrations along the flow paths of deep waters in the Southwest Atlantic. Earth
676 Planet. Sci. Lett. 390, 93-102.

677 Edwards, R.L., Chen, J.H. and Wasserburg, G.J. (1987) ^{238}U-^{234}U-^{230}Th-^{232}Th systematics and the precise
678 measurement of time over the past 500,000 years. Earth Planet. Sci. Lett. 81, 175-192.

679 Fitzsimmons, J.N. and Boyle, E.A. (2014a) Assessment and comparison of Anopore and cross flow
680 filtration methods for the determination of dissolved iron size fractionation into soluble and colloidal
681 phases in seawater. Limnol. Oceanogr. Methods 12, 246-263.

682 Fitzsimmons, J.N. and Boyle, E.A. (2014b) Both soluble and colloidal iron phases control dissolved iron
683 variability in the tropical North Atlantic Ocean. Geochim. Cosmochim. Acta 125, 539-550.

684 Fitzsimmons, J.N., Boyle, E.A., Hatta, M. and Wu, J. (in press) Partitioning of dissolved iron and iron
685 isotopes into soluble and colloidal phases along the GA03 GEOTRACES North Atlantic Transect. Deep-
686 Sea Res. II.

687 Fitzsimmons, J.N., Hayes, C.T., al-Subiai, S., Morton, P.L., Weisend, R., Ascani, F. and Boyle, E.A.
688 (submitted) Daily to decadal variability of size-fractionated iron and iron-binding ligands at the Hawaii
689 Ocean Time-series Station ALOHA. Geochim. Cosmochim. Acta.

690 Gledhill, M. and Buck, K.N. (2012) The organic complexation of iron in the marine environment: A
691 review. Front. Microbiol. 3.

692 Guo, L. and Santschi, P.H. (2007) Ultrafiltration and its applications to sampling and characterisation of
693 aquatic colloids. IUPAC Series on Analytical and Physical Chemistry of Environmental Systems 10, 159.

694 Guo, L., Santschi, P.H. and Baskaran, M. (1997) Interactions of thorium isotopes with colloidal organic
695 matter in oceanic environments. Colloids Surf. A 120, 255-271.

696 Hayes, C.T., Anderson, R.F., Fleisher, M.Q., Huang, K.-F., Robinson, L.F., Lu, Y., Cheng, H., Edwards,
697 R.L. and Moran, S.B. (2014) ^{230}Th and ^{231}Pa on GEOTRACES GA03, the U.S. GEOTRACES North
698 Atlantic transect, and implications for modern and paleoceanographic chemical fluxes. Deep-Sea Res. II.

699 Hayes, C.T., Anderson, R.F., Fleisher, M.Q., Lam, P.J., Ohnemus, D.C., Huang, K.-F., Robinson, L.F.,
700 Lu, Y., Cheng, H., Edwards, R.L. and Moran, S.B. (submitted) Intensity of Th and Pa scavenging
701 partitioned by particle chemistry in the North Atlantic Ocean. Mar. Chem.

702 Hayes, C.T., Anderson, R.F., Fleisher, M.Q., Serno, S., Winckler, G. and Gersonde, R. (2013a)
703 Quantifying lithogenic inputs to the North Pacific Ocean using the long-lived thorium isotopes. Earth
704 Planet. Sci. Lett. 383, 16-25.

705 Hayes, C.T., Anderson, R.F., Jaccard, S.L., François, R., Fleisher, M.Q., Soon, M. and Gersonde, R.
706 (2013b) A new perspective on boundary scavenging in the North Pacific Ocean. Earth Planet. Sci. Lett.
707 369-370, 86-97.

708 Hirose, K. (2004) Chemical Speciation of Thorium in Marine Biogenic Particulate Matter.
709 TheScientificWorldJOURNAL 4, 67-76.

710 Ho, T.-Y., Chou, W.-C., Lin, H.-L. and Sheu, D.D. (2011) Trace metal cycling in the deep water of the
711 South China Sea: The composition, sources, and fluxes of sinking particles. Limnol. Oceanogr. 56, 1225-
712 1243.

713 Honeyman, B.D., Balistrieri, L.S. and Murray, J.W. (1988) Oceanic trace metal scavenging: the
714 importance of particle concentration. Deep-Sea Res. A 35, 227-246.

715 Honeyman, B.D. and Santschi, P.H. (1989) A Brownian-pumping model for oceanic trace metal
716 scavenging: Evidence from Th isotopes. J. Mar. Res. 47, 951-992.

717 Hsieh, Y.-T., Henderson, G.M. and Thomas, A.L. (2011) Combining seawater ^{232}Th and ^{230}Th
718 concentrations to determine dust fluxes to the surface ocean. Earth Planet. Sci. Lett. 312, 280-290.

719 Huh, C.-A. and Prahl, F.G. (1995) Role of colloids in upper ocean biogeochemistry in the northeast
720 Pacific Ocean elucidated from ^{238}U-^{234}Th disequilibria. Limnol. Oceanogr. 40, 528-528.

721 Hyslop, N.P., Trzepla, K., Wallis, C.D., Matzoll, A.K. and White, W.H. (2013) Technical note: A 23-year
722 record of twice-weekly aerosol composition measurements at Mauna Loa Observatory. Atmos. Environ.
723 80, 259-263.

724 Jickells, T.D. (1999) The inputs of dust derived elements to the Sargasso Sea; a synthesis. Mar. Chem. 68,
725 5-14.

726 Jickells, T.D., An, Z.S., Andersen, K.K., Baker, A.R., Bergametti, G., Brooks, N., Cao, J.J., Boyd, P.W.,
727 Duce, R.A., Hunter, K.A., Kawahata, H., Kubilay, N., laRoche, J., Liss, P.S., Mahowald, N., Prospero,
728 J.M., Ridgwell, A.J., Tegen, I. and Torres, R. (2005) Global iron connections between desert dust, ocean
729 biogeochemistry, and climate. Science 308, 67-71.

730 Karl, D.M., Church, M.J., Dore, J.E., Letelier, R.M. and Mahaffey, C. (2012) Predictable and efficient
731 carbon sequestration in the North Pacific Ocean supported by symbiotic nitrogen fixation. Proc. Natl.
732 Acad. Sci. U. S. A.

733 Karl, D.M. and Lukas, R. (1996) The Hawaii Ocean Time-series (HOT) program: Background, rationale
734 and field implementation. Deep-Sea Res. II 43, 129-156.

735 Kitayama, S., Kuma, K., Manabe, E., Sugie, K., Takata, H., Isoda, Y., Toya, K., Saitoh, S.-i., Takagi, S.,
736 Kamei, Y. and Sakaoka, K. (2009) Controls on iron distributions in the deep water column of the North
737 Pacific Ocean: Iron(III) hydroxide solubility and marine humic-type dissolved organic matter. J.
738 Geophys. Res. 114, C08019.

739 Kuma, K., Isoda, Y. and Nakabayashi, S. (2003) Control on dissolved iron concentrations in deep waters
740 in the western North Pacific: Iron(III) hydroxide solubility. J. Geophys. Res. 108, 3289.

741 Kuma, K., Nishioka, J. and Matsunaga, K. (1996) Controls on iron(III) hydroxide solubility in seawater:
742 the influence of pH and natural organic chelators. Limnol. Oceanogr. 41, 396-407.

743 Lee, J.-M., Boyle, E.A., Echegoyen-Sanz, Y., Fitzsimmons, J.N., Zhang, R. and Kayser, R.A. (2011)
744 Analysis of trace metals (Cu, Cd, Pb, and Fe) in seawater using single batch nitrilotriacetate resin
745 extraction and isotope dilution inductively coupled plasma mass spectrometry. Anal. Chim. Acta 686, 93-
746 101.

747 Lehnert, K., Su, Y., Langmuir, C.H., Sarbas, B. and Nohl, U. (2000) A global geochemical database
748 structure for rocks. Geochemistry, Geophysics, Geosystems 1, 1012.

749 Liu, X. and Millero, F.J. (2002) The solubility of iron in seawater. Mar. Chem. 77, 43-54.

Luo, S., Ku, T.-L., Kusakabe, M., Bishop, J.K.B. and Yang, Y.-L. (1995) Tracing particle cycling in the upper ocean with ^{230}Th and ^{228}Th: An investigation in the equatorial Pacific along 140°W. Deep-Sea Res. II 42, 805-829.

Mahowald, N.M., Baker, A.R., Bergametti, G., Brooks, N., Duce, R.A., Jickells, T.D., Kubilay, N., Prospero, J.M. and Tegen, I. (2005) Atmospheric global dust cycle and iron inputs to the ocean. Global Biogeochem. Cycles 19, GB4025.

Martínez-García, A., Sigman, D.M., Ren, H., Anderson, R.F., Straub, M., Hodell, D.A., Jaccard, S.L., Eglinton, T.I. and Haug, G.H. (2014) Iron Fertilization of the Subantarctic Ocean During the Last Ice Age. Science 343, 1347-1350.

McCave, I.N. (1986) Local and global aspects of the bottom nepheloid layers in the world ocean. Neth. J. Sea Res. 20, 167-181.

McGee, D. (2009) Reconstructing and interpreting the dust record and probing the plumbing of Mono Lake. PhD dissert. Columbia University, New York, NY.

Mendez, J., Guieu, C. and Adkins, J. (2010) Atmospheric input of manganese and iron to the ocean: Seawater dissolution experiments with Saharan and North American dusts. Mar. Chem. 120, 34-43.

Moore, C.M., Mills, M.M., Arrigo, K.R., Berman-Frank, I., Bopp, L., Boyd, P.W., Galbraith, E.D., Geider, R.J., Guieu, C., Jaccard, S.L., Jickells, T.D., La Roche, J., Lenton, T.M., Mahowald, N.M., Maranon, E., Marinov, I., Moore, J.K., Nakatsuka, T., Oschlies, A., Saito, M.A., Thingstad, T.F., Tsuda, A. and Ulloa, O. (2013) Processes and patterns of oceanic nutrient limitation. Nature Geosci. 6, 701-710.

Moran, S.B. and Buesseler, K.O. (1992) Short residence time of colloids in the upper ocean estimated from ^{238}U-^{234}Th disequilibria. Nature 359, 221-223.

Morton, P.L. (2010) Trace metal biogeochemistry in the western North Pacific, PhD Dissert. Old Dominion University, Norfolk, VA.

Morton, P.L., Landing, W.M., Hsu, S.-C., Milne, A., Aguilar-Islas, A.M., Baker, A.R., Bowie, A.R., Buck, C.S., Gao, Y., Gichuki, S., Hastings, M.G., Hatta, M., Johansen, A.M., Losno, R., Mead, C., Patay, M.D., Swarr, G., Vendermark, A. and Zamora, L.M. (2013) Methods for sampling and analysis of marine aerosols: results from the 2008 GEOTRACES aerosol intercalibration experiment. Limnol. Oceanogr. Methods 11, 62-78.

Neck, V., Altmaier, M., Müller, R., Bauer, A., Fanghänel, T. and Kim, J.-I. (2003) Solubility of crystalline thorium dioxide. Radiochim. Acta 91.

Ohnemus, D.C. and Lam, P.J. (in press) Cycling of lithogenic marine particulates in the US GEOTRACES North Atlantic Zonal Transect. Deep-Sea Res. II.

Okubo, A., Obata, H., Gamo, T. and Yamada, M. (2012) ^{230}Th and ^{232}Th distributions in mid-latitudes of the North Pacific Ocean: Effect of bottom scavenging. Earth Planet. Sci. Lett. 339–340, 139-150.

Owens, S.A., Buesseler, K.O. and Sims, K.W.W. (2011) Re-evaluating the ^{238}U-salinity relationship in seawater: Implications for the ^{238}U–^{234}Th disequilibrium method. Mar. Chem. 127, 31-39.

786 Prospero, J.M., Savoie, D.L. and Arimoto, R. (2003) Long-term record of nss-sulfate and nitrate in
787 aerosols on Midway Island, 1981–2000: Evidence of increased (now decreasing?) anthropogenic
788 emissions from Asia. J. Geophy. Res. 108, 4019.

789 Reuer, M.K., Boyle, E.A. and Grant, B.C. (2003) Lead isotope analysis of marine carbonates and
790 seawater by multiple collector ICP-MS. Chem. Geol. 200, 137-153.

791 Richards, K.J. (1990) Physical processes in the benthic boundary layer. Philos. Trans. R. Soc. London,
792 Ser. A 331, 3-13.

793 Roy-Barman, M., Chen, J.H. and Wasserburg, G.J. (1996) ^{230}Th-^{232}Th systematics in the central Pacific
794 Ocean: The sources and the fates of thorium. Earth Planet. Sci. Lett. 139, 351-363.

795 Roy-Barman, M., Coppola, L. and Souhaut, M. (2002) Thorium isotopes in the western Mediterranean
796 Sea: an insight into the marine particle dynamics. Earth Planet. Sci. Lett. 196, 161-174.

797 Roy-Barman, M., Lemaître, C., Ayrault, S., Jeandel, C., Souhaut, M. and Miquel, J.C. (2009) The
798 influence of particle composition on thorium scavenging in the Mediterranean Sea. Earth Planet. Sci. Lett.
799 286, 526-534.

800 Rubin, M., Berman-Frank, I. and Shaked, Y. (2011) Dust- and mineral-iron utilization by the marine
801 dinitrogen-fixer Trichodesmium. Nature Geosci. 4, 529-534.

802 Rue, E.L. and Bruland, K.W. (1995) Complexation of iron(III) by natural organic ligands in the Central
803 North Pacific as determined by a new competitive ligand equilibration/adsorptive cathodic stripping
804 voltammetric method. Mar. Chem. 50, 117-138.

805 Santschi, P.H., Murray, J.W., Baskaran, M., Benitez-Nelson, C.R., Guo, L.D., Hung, C.C., Lamborg, C.,
806 Moran, S.B., Passow, U. and Roy-Barman, M. (2006) Thorium speciation in seawater. Mar. Chem. 100,
807 250-268.

808 Schlosser, C. and Croot, P. (2008) Application of cross-flow filtration for determining the solubility of
809 iron species in open ocean seawater. Limnol. Oceanogr. Methods 6, 630-642.

810 Serno, S., Winckler, G., Anderson, R.F., Hayes, C.T., McGee, D., Machalett, B., Ren, H., Straub, S.M.,
811 Gersonde, R. and Haug, G.H. (2014) Eolian dust input to the Subarctic North Pacific. Earth Planet. Sci.
812 Lett. 387, 252-263.

813 Tagliabue, A., Aumont, O. and Bopp, L. (2014) The impact of different external sources of iron on the
814 global carbon cycle. Geophys. Res. Lett. 41, 2013GL059059.

815 Taylor, S.R. and McLennan, S.M. (1995) The geochemical evolution of the continental crust. Rev.
816 Geophys. 33, 241-265.

817 Upadhyay, N., Majestic, B.J., Prapaipong, P. and Herckes, P. (2009) Evaluation of polyurethane foam,
818 polypropylene, quartz fiber, and cellulose substrates for multi-element analysis of atmospheric particulate
819 matter by ICP-MS. Anal. Bioanal. Chem. 394, 255-266.

820 Ussher, S.J., Achterberg, E.P., Powell, C., Baker, A.R., Jickells, T.D., Torres, R. and Worsfold, P.J.
821 (2013) Impact of atmospheric deposition on the contrasting iron biogeochemistry of the North and South
822 Atlantic Ocean. Global Biogeochem. Cycles 27, 1096-1107.

823 Ward, B.A., Dutkiewicz, S., Moore, C.M. and Follows, M.J. (2013) Iron, phosphorus, and nitrogen
824 supply ratios define the biogeography of nitrogen fixation. Limnol. Oceanogr. 58, 2059-2075.
825
826

Figure 1

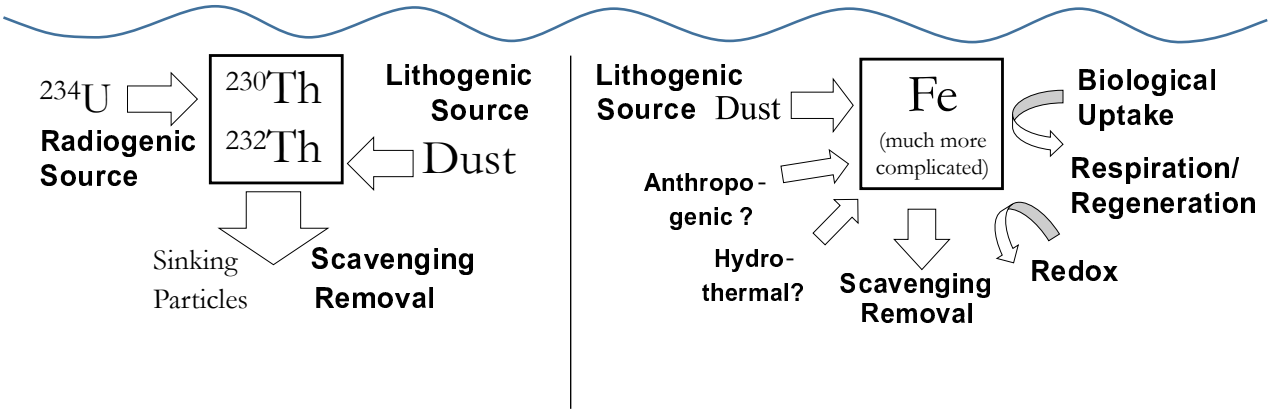
234U
Radiogenic Source
230Th
232Th
Lithogenic Source
Dust
Sinking Particles
Scavenging Removal
Lithogenic Source
Dust
Fe
(much more complicated)
Biological Uptake
Respiration/ Regeneration
Anthropo-genic ?
Hydro-thermal?
Scavenging Removal
Redox

Figure 2

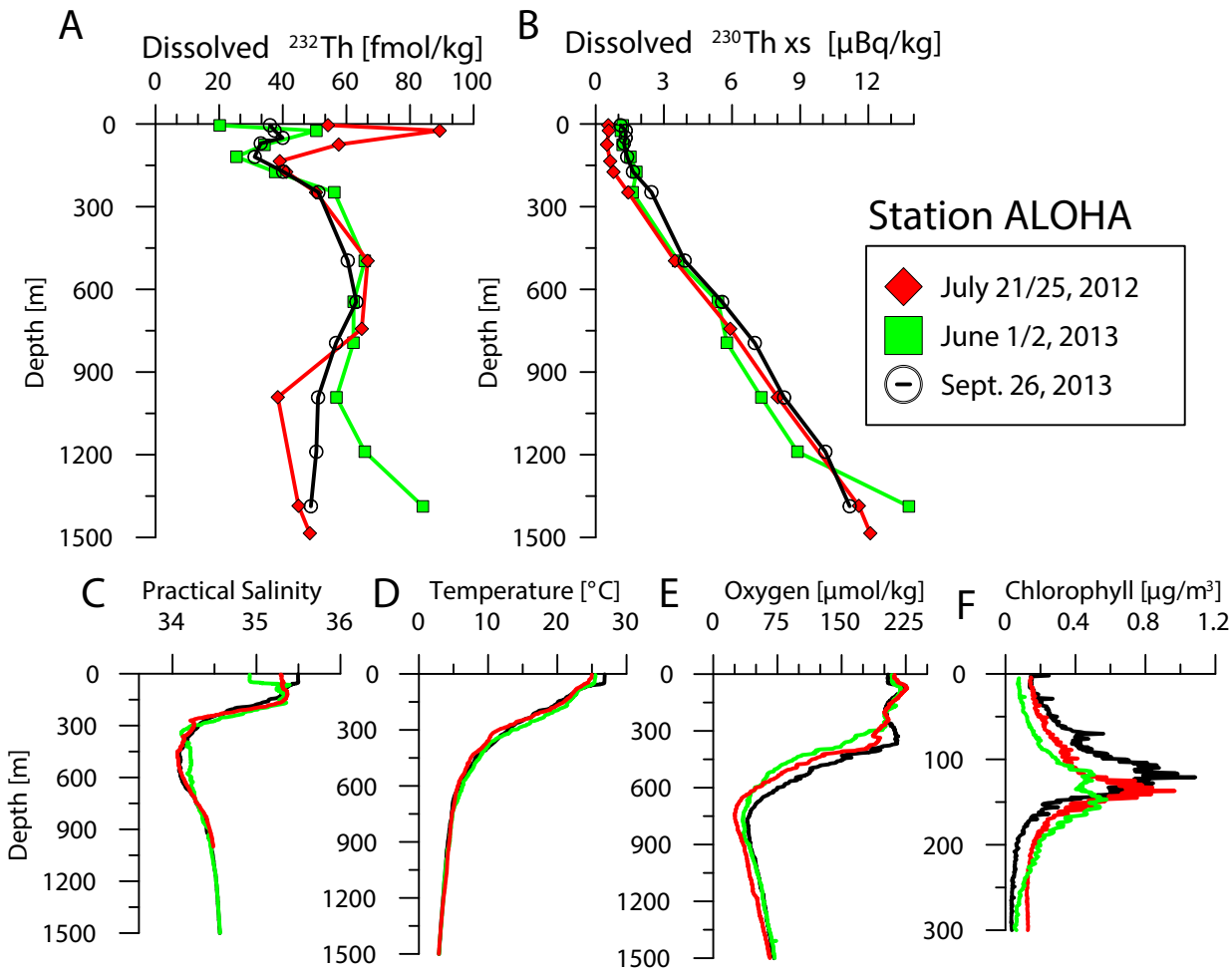
A
Dissolved ^{232}Th [fmol/kg]
0 20 40 60 80 100
B
Dissolved ^{230}Th xs [µBq/kg]
0 3 6 9 12
Depth [m]
0 300 600 900 1200 1500
Station ALOHA
July 21/25, 2012
June 1/2, 2013
Sept. 26, 2013
C
Practical Salinity
34 35 36
D
Temperature [°C]
0 10 20 30
E
Oxygen [µmol/kg]
0 75 150 225
F
Chlorophyll [µg/m³]
0 0.4 0.8 1.2
0 100 200 300

Figure 3

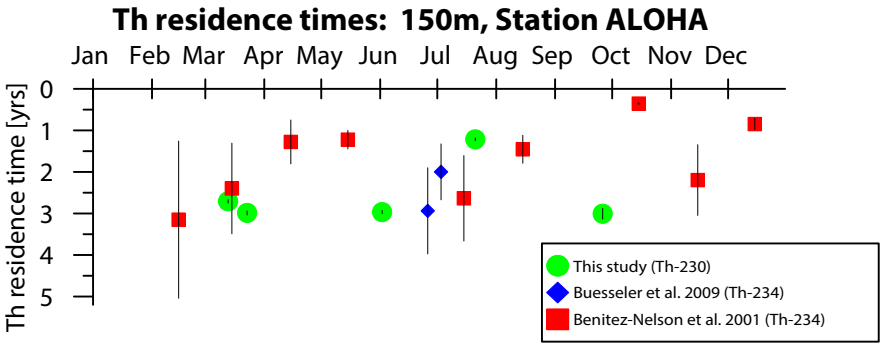
Th residence times: 150m, Station ALOHA
Jan
Feb
Mar
Apr
May
Jun
Jul
Aug
Sep
Oct
Nov
Dec
Th residence time [yrs]
0
1
2
3
4
5
This study (Th-230)
Buesseler et al. 2009 (Th-234)
Benitez-Nelson et al. 2001 (Th-234)

Figure 4

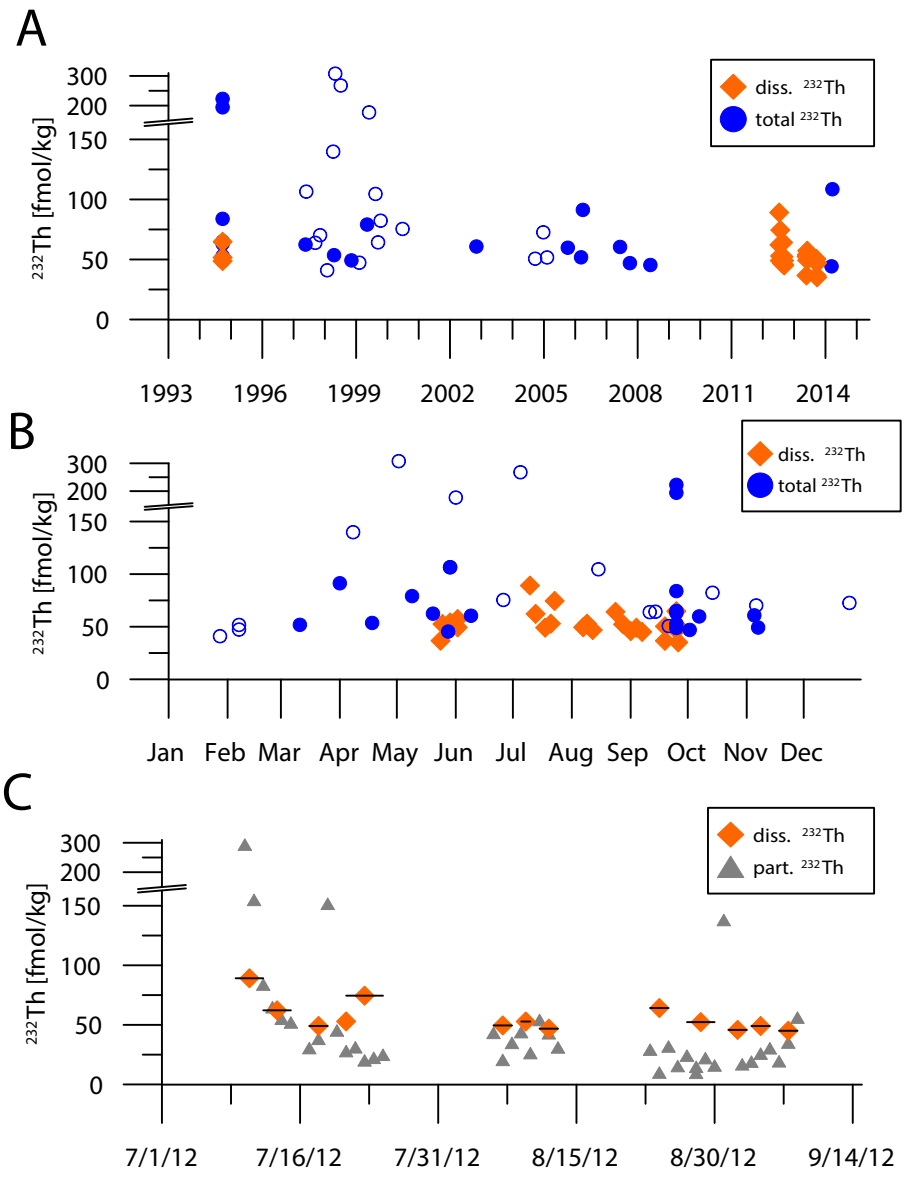
A
300
200
150
100
50
0
232Th [fmol/kg]
diss. 232Th
total 232Th
1993
1996
1999
2002
2005
2008
2011
2014
B
300
200
150
100
50
0
232Th [fmol/kg]
diss. 232Th
total 232Th
Jan
Feb
Mar
Apr
May
Jun
Jul
Aug
Sep
Oct
Nov
Dec
C
300
200
150
100
50
0
232Th [fmol/kg]
diss. 232Th
part. 232Th
7/1/12
7/16/12
7/31/12
8/15/12
8/30/12
9/14/12

Figure 5

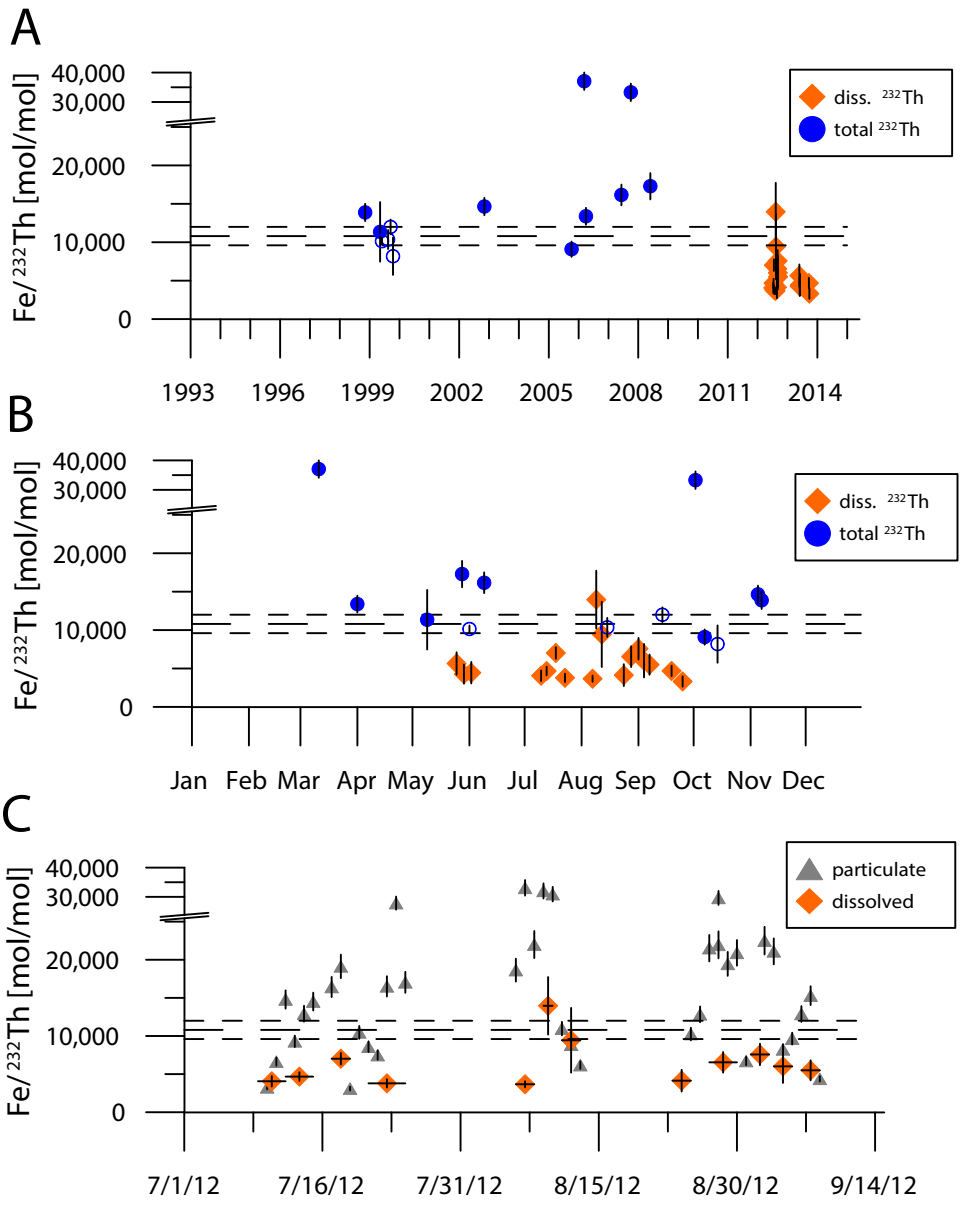
A
40,000
30,000
20,000
10,000
0
Fe/232Th [mol/mol]
diss. 232Th
total 232Th
1993
1996
1999
2002
2005
2008
2011
2014
B
40,000
30,000
20,000
10,000
0
Fe/232Th [mol/mol]
diss. 232Th
total 232Th
Jan
Feb
Mar
Apr
May
Jun
Jul
Aug
Sep
Oct
Nov
Dec
C
40,000
30,000
20,000
10,000
0
Fe/232Th [mol/mol]
particulate
dissolved
7/1/12
7/16/12
7/31/12
8/15/12
8/30/12
9/14/12

Figure 6

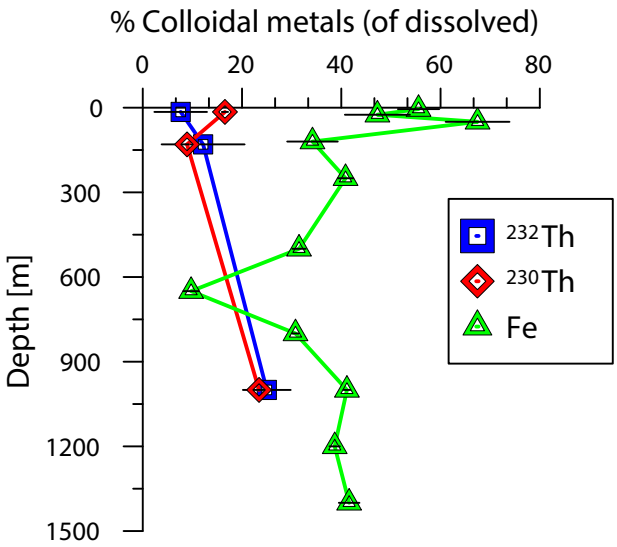
% Colloidal metals (of dissolved)
0
20
40
60
80
0
300
600
900
1200
1500
Depth [m]
232Th
230Th
Fe

Figure 7

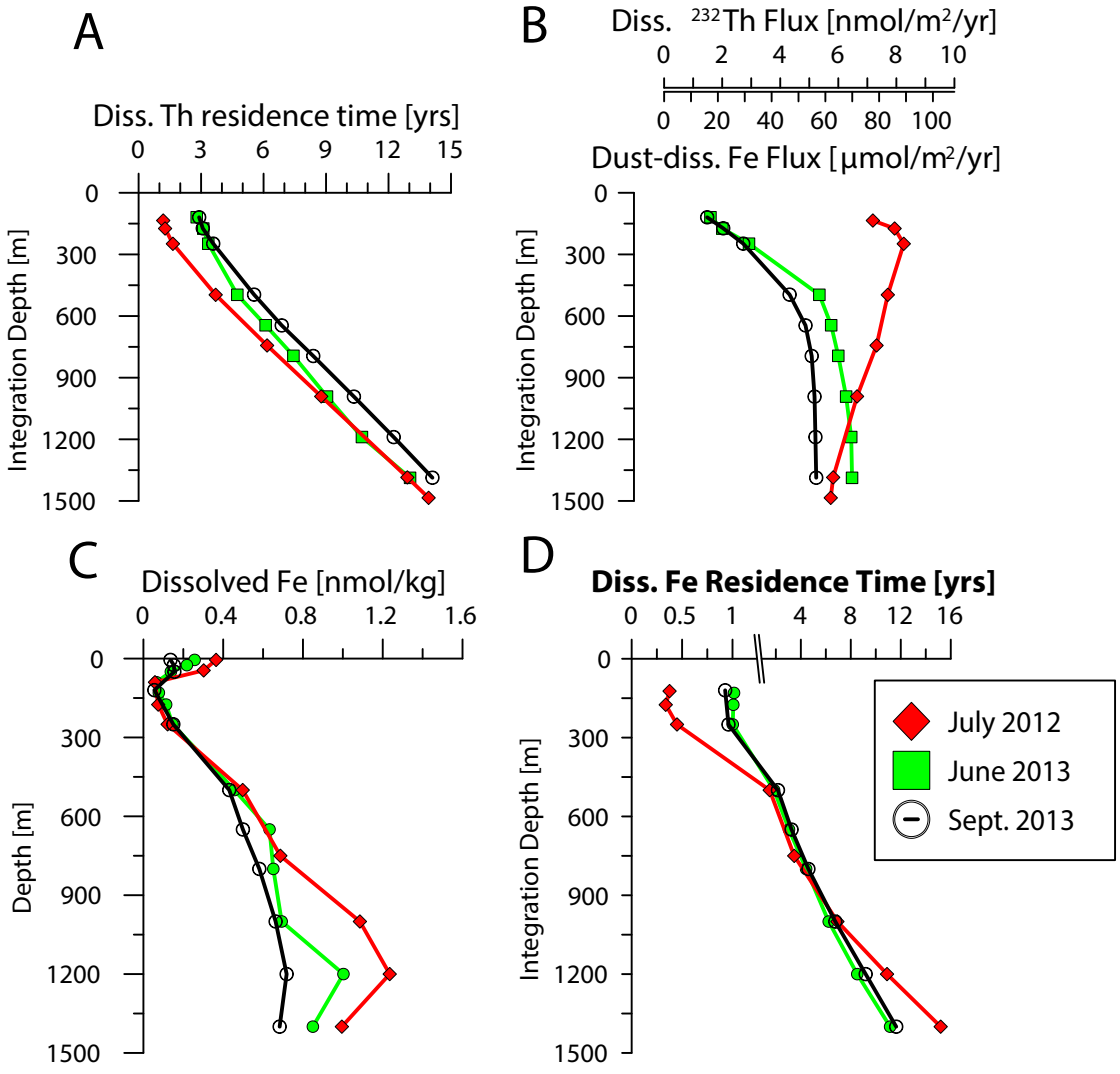
A
Diss. Th residence time [yrs]
0 3 6 9 12 15
Integration Depth [m]
0 300 600 900 1200 1500
B
Diss. 232Th Flux [nmol/m2/yr]
0 2 4 6 8 10
0 20 40 60 80 100
Dust-diss. Fe Flux [µmol/m2/yr]
Integration Depth [m]
0 300 600 900 1200 1500
C
Dissolved Fe [nmol/kg]
0 0.4 0.8 1.2 1.6
Depth [m]
0 300 600 900 1200 1500
D
Diss. Fe Residence Time [yrs]
0 0.5 1 4 8 12 16
Integration Depth [m]
0 300 600 900 1200 1500
July 2012
June 2013
Sept. 2013

Figure 8

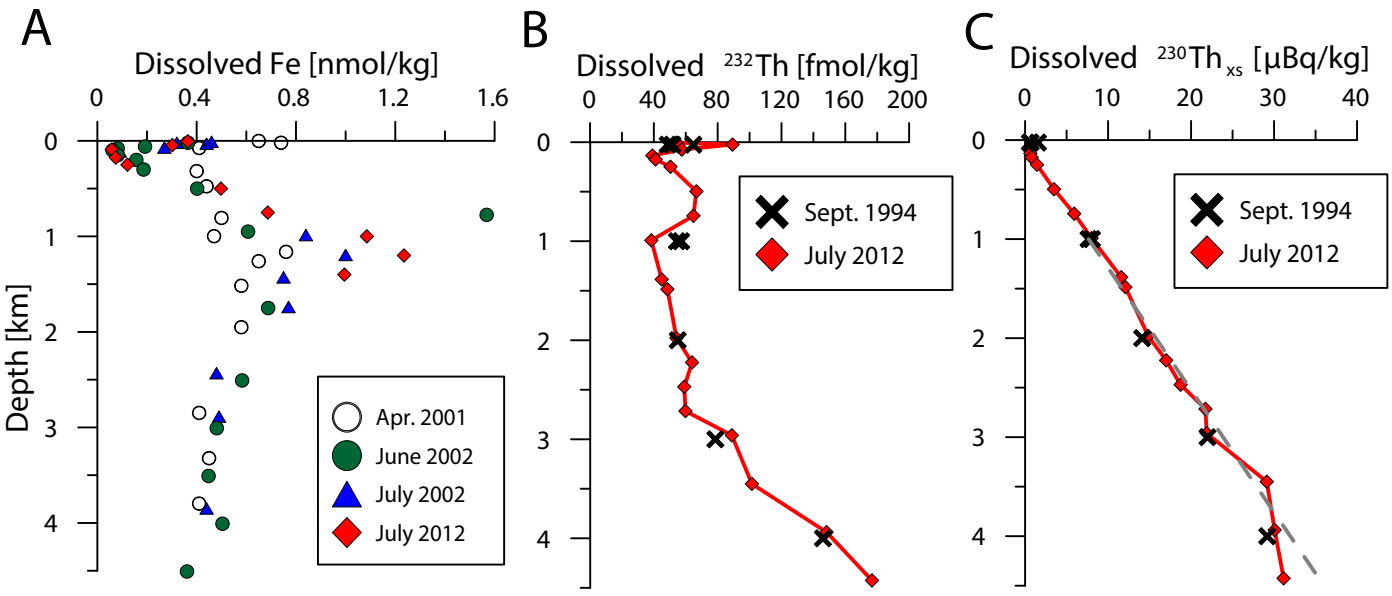
A
Dissolved Fe [nmol/kg]
0
0.4
0.8
1.2
1.6
Depth [km]
0
1
2
3
4
Apr. 2001
June 2002
July 2002
July 2012
B
Dissolved 232Th [fmol/kg]
0
40
80
120
160
200
Sept. 1994
July 2012
C
Dissolved 230Th xs [µBq/kg]
0
10
20
30
40
Sept. 1994
July 2012

Figure 9

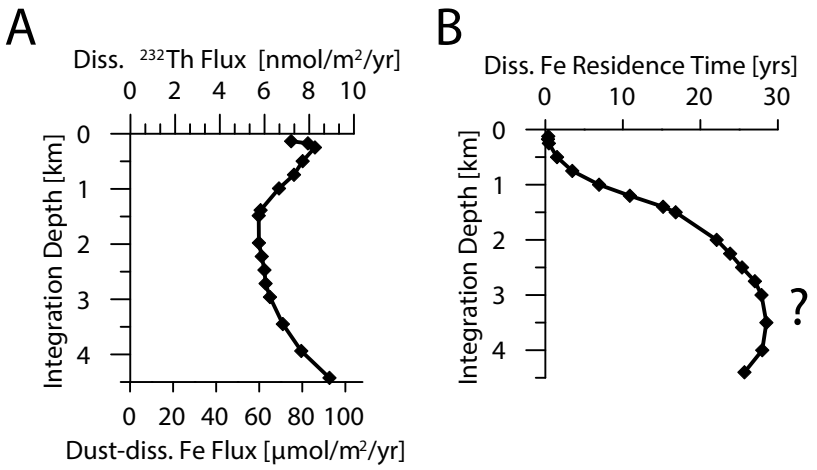
A
Diss. 232Th Flux [nmol/m2/yr]
0 2 4 6 8 10
Integration Depth [km]
0
1
2
3
4
0 20 40 60 80 100
Dust-diss. Fe Flux [µmol/m2/yr]
B
Diss. Fe Residence Time [yrs]
0 10 20 30
Integration Depth [km]
0
1
2
3
4
?

Electronic Annex

Click here to download Electronic Annex: Hayes ALOHA Th Fe Supplemental Data for GCA.xlsx